Conformation and elasticity of the isolated red blood cell membrane skeleton

Karel Svoboda,*‡ Christoph F. Schmidt,*§‖ Daniel Branton,‡ and Steven M. Block‡§
*Departments of Physics, and ‡Cellular and Developmental Biology, Harvard University, Cambridge, Massachusetts 02138; and
§Rowland Institute for Science, Cambridge, Massachusetts 02142 USA

ABSTRACT We studied the structure and elasticity of membrane skeletons from human red blood cells (RBCs) during and after extraction of RBC ghosts with nonionic detergent. Optical tweezers were used to suspend individual cells inside a flow chamber, away from all surfaces; this procedure allowed complete exchange of medium while the low-contrast protein network of the skeleton was observed by high resolution, video-enhanced differential interference-contrast (DIC) microscopy. Immediately following extraction in a 5 mM salt buffer, skeletons assumed expanded, nearly spherical shapes that were uncorrelated with the shapes of their parent RBCs. Judging by the extent of thermal undulations and by their deformability in small flow fields, the bending rigidity of skeletons was markedly lower than that of either RBCs or ghosts. No further changes were apparent in skeletons maintained in this buffer for up to 40 min at low temperatures ($T < 10°C$), but skeletons shrank when the ionic strength of the buffer was increased. When the salt concentration was raised to 1.5 M, shrinkage remained reversible for ~1 min but thereafter became irreversible. When maintained in 1.5 M salt buffer for longer periods, skeletons continued to shrink, lost flexibility, and assumed irregular shapes: this rigidification was irreversible. At this stage, skeletons closely resembled those isolated in standard bulk preparations. We propose that the transformation to the rigid, irreversibly shrunken state is a consequence of spectrin dimer-dimer reconnections and that these structural rearrangements are thermally activated. We also measured the salt-dependent size of fresh and bulk extracted skeletons. Our measurements suggest that, in situ, the spectrin tethers are flexible, with a persistence length of ~10 nm at 150 mM salt.

INTRODUCTION

An important determinant of the mechanical properties of mammalian red blood cells is a semiregular, relatively stable, cross-linked network of proteins—the membrane skeleton—that lines the cytoplasmic side of the cell membrane (Elgsaeter et al., 1986; Steck, 1989; Bennett, 1990). Studies of abnormal RBCs (Chasis and Mohandas, 1986; Waugh, 1987; Waugh and Agre, 1988) have shown that the membrane skeleton provides for shear elasticity (Evans, 1973) and prevents membrane loss (blebbing) during the large deformations to which mammalian erythrocytes are subject while circulating through the cardiovascular system.

The lipid of the cell membrane can be dissolved by detergent treatment, leaving behind an extracted membrane skeleton (Yu et al., 1973). Electron microscopy of skeletons has revealed a remarkable two-dimensional, triangulated lattice composed of spectrin tetramers that are cross-linked by junctions containing rods of polymeric actin (Byers and Branton, 1986; Liu et al., 1987). Electron microscopic and viscometric studies suggest that isolated spectrin tetramers, under isotonic conditions, have a short persistence length (de Gennes, 1979; Flory, 1988) compared with their overall contour length (Shotton et al., 1979; Stokke et al., 1985). Consequently, while acting as tethers in the skeleton network, spectrin molecules are expected to show random coil conformations and dynamics, despite some evidence from electron micrographs indicating that spectrin, in situ, might be stiff (McGough and Josephs, 1990).

Skeletons can expand or shrink with changing ionic strength, pH, temperature, or concentration of a denaturant (Johnson et al., 1980; Lange et al., 1982; Vertessy and Steck, 1989). Detergent-extracted skeletons reportedly exhibit shape memory, implying that the skeletal structure, whose elements are in a slow association equilibrium with each other, is continuously imprinted with the contour of the cell and is able to maintain that contour over short time scales (Lange et al., 1982; Steck, 1989). But the skeletons used in these reports were observed hours or days after extraction, at times when the skeleton's mechanical properties might no longer reflect those in vivo. Here, we observed the evolution of skeletons at the time of extraction, using optical tweezers to suspend individual cells inside a flow chamber in such a way that the dissolution of the lipid bilayer and the properties of the extracted skeleton could be observed directly with high resolution microscopy. We found that within minutes of extraction the skeletons underwent salt- and temperature-dependent changes. We believe that these are a consequence of spectrin dimer-dimer reconnections that can be facilitated by salt-dependent shifts of the dimer-tetramer equilibrium.

MATERIALS AND METHODS

Chemicals

Dithiothreitol, adenosine triphosphate (ATP),[1] and ethyleneglycol-bis(β-aminoethyl ether)-*N,N,N′,N′*-tetraacetic acid (EGTA) were ob-

‖ Address correspondence to Christoph F. Schmidt, Rowland Institute for Science, 100 Cambridge Parkway, Cambridge, Massachusetts 02142.

[1] Abbreviations used in this paper: ATP, adenosine triphosphate; BSA, bovine serum albumin; EGTA, ethyleneglycol-bis(β-aminoethyl ether)-*N,N,N′,N′*-tetraacetic acid; RBC, red blood cell.

0006-3495/92/09/784/10 $2.00

tained from Sigma Chemical Co. (St. Louis, MO), bovine serum albumin (BSA) from ICN Biomedicals Inc. (Costa Mesa, CA), and Triton X-100 from EM Science (Gibbstown, NJ). All other chemicals were reagent grade.

Buffers

Solutions were prepared from microfiltered, deionized water (R > 10 MΩ/cm). Except where otherwise specified, buffers were based on 5 mM Na-phosphate (pH 7.6), 0.1 mM $MgSO_4$, 0.1 mM EGTA, 1 mg/ml BSA, and 1 mM dithiothreitol, to which NaCl was added to achieve the specified salt concentrations > 5 mM. Water was added to achieve salt concentrations below 5 mM. Hypotonic buffers (<150 mM NaCl) contained 0.1 mM ATP and 0.2 mM NaN_3. Isotonic and hypertonic buffers (>150 mM NaCl) contained 1 mM ATP and 2 mM NaN_3. To extract skeletons, Triton X-100 (1% wt/vol) was added to the buffer of the desired salt concentration. All buffers after extraction contained the same 1% wt/vol concentration of detergent.

Microscopy

Specimens were viewed with high resolution differential interference-contrast video microscopy in a modified microscope (Axiovert 35, Carl Zeiss, Oberkochen, Germany) equipped with a 100X Plan Neofluar oil-immersion objective (1.30 NA), an aplanatic oil-immersion condenser (1.40 NA), and a mercury arc lamp (Osram HBO 100W/2; Carl Zeiss) attached to a fiberoptic scrambler of the Ellis type (Instrument Development Laboratory, Woods Hole, MA). Video-enhanced microscopy and digital image processing were performed as described previously (Block et al., 1991). Images were recorded on a Hi-8 videocassette recorder (model EVO-9700; Sony Corp. of America, Teaneck, NJ) or an optical memory disk recorder (Panasonic model TQ-2028F; Matsushita Electric Corp. of America, Secaucus, NJ), and hardcopy was produced with a video graphic printer (model UP-850; Sony Corp. of America, Teaneck, NJ). The microscope stage was thermostatically controlled by a Peltier device, and the microscope objective was maintained at the same temperature by means of a brass jacket connected to a recirculating water bath (Lauda RMS-6; Brinkman Instruments, Inc., Westbury, NY). For low-temperature experiments, samples and buffers were kept on ice before use. To facilitate rapid exchange of media, we used a miniature flow chamber developed for this purpose (Berg and Block, 1984) and equipped with polyethylene tubing (PE-50, 0.58 mm ID; Clay-Adams Division of Becton Dickinson, Parsippany, NJ). Inlet tubes were kept short (<10 cm) to minimize fluid exchange time, and buffers and samples were held in a miniature tube rack attached to the microscope stage. Solutions were pumped at constant, reproducible rates using a programmable syringe pump (Pump 22; Harvard Apparatus, South Natick, MA) connected by an RS-232C interface to a laptop computer and driven by custom software.

Optical tweezers

Optical tweezers consists of single-beam gradient force optical trap, formed by light from a laser brought to a diffraction-limited spot by a microscope objective of high numerical aperture (Ashkin et al., 1986; for a review, see Block, 1990). The intense electromagnetic field gradient in the vicinity of the focus is able to trap microscopic, refractile particles by radiation pressure (Fig. 1). We used an infrared laser (Nd:YAG, λ = 1,064 nm, 1W CW, model C-95 YAGMAX; CVI Lasers, Albuquerque, NM) that is capable of manipulating living material nondestructively; particular features of our setup have been described elsewhere (Block, 1990). External optics were used to position the trap anywhere within the field of view of the microscope. Most commonly, the axial (z-) position of the trap was adjusted to be parfocal with the specimen plane, and the lateral (x- and y-) controls were used to maneuver the object of interest in the video field. In certain cases, the axial position was positioned above or below the specimen plane to bring other parts of a larger object into focus.

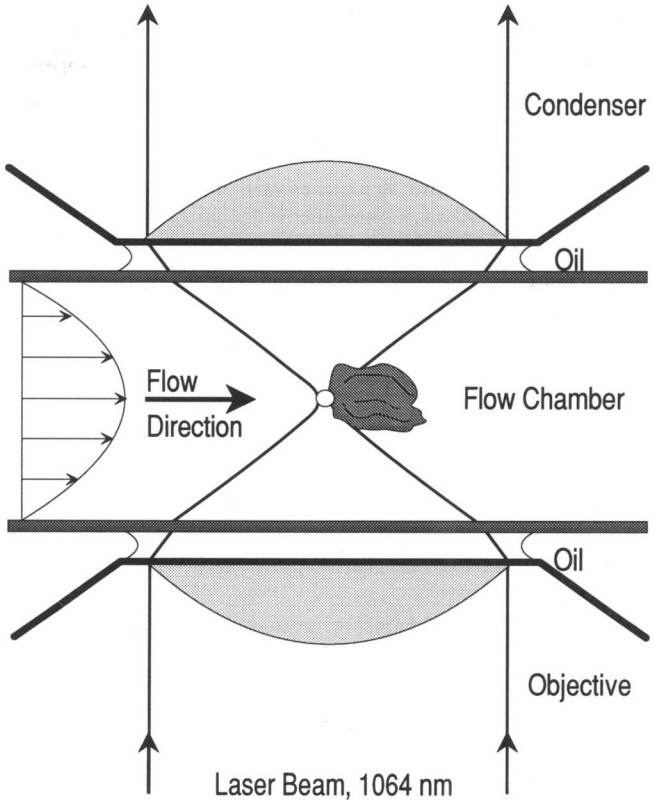

FIGURE 1 A cartoon (not to scale) of a membrane skeleton suspended inside a flow chamber, using optical tweezers to grasp an attached silica bead. An inverted microscope configuration using oil-immersion optics is shown. The diagram illustrates the parabolic flow profile of buffer in the chamber (*left*) and the laser light forming the trap (*center*). The objective focuses the laser beam to a diffraction-limited beam waist ~1 μm in diameter, in which dielectric particles, such as the silica bead, are strongly trapped. Buffer can be pumped past the stationary skeleton at flow velocities up to 100 μm/s, permitting complete medium exchange within 60 s. The overall depth of the actual chamber is ~350 μm, and skeletons were typically held ~10 μm above the lower coverglass of the chamber.

Skeleton morphometry

The shallow depth of field of differential interference-contrast microscopy (~0.3 μm) made it possible to image optical cross-sections of skeletons; the extent and the shape of skeletons along the optical axis were determined by systematically focusing through the objects. During most video recording, specimens were positioned using optical tweezers and the microscope was focused on the central cross section of a skeleton. Circumferences of skeletons were traced and measured from still frames of recorded data using a digital image processor (IMAGE 1; Universal Imaging Corp., West Chester, PA). Skeleton circumferences were measured mainly at zero, but occasionally at reduced, buffer flow rates (<10 μm/s in the focal plane; such reduced rates did not alter the measured circumferences, as was verified in a number of cases by comparing values obtained at zero and reduced flow rates). To minimize the effects of thermal fluctuations, circumferences were averaged for a minimum of three still frames obtained for each skeleton at a given salt concentration. The values from several such skeletons were then averaged to produce a mean circumference; the diameter for an equivalent sphere was calculated by dividing the mean circumference by π. This "equivalent sphere diameter" gave a more reliable value than a direct measurement of the diameter, because skeletons, especially those prepared by the bulk method, often showed

TABLE 1

Sample	Equivalent diameter*	Average tether length	Equivalent surface area	Flexibility‡
	μm	nm	μm^2	
Ghosts in 5 mM salt, $T \leq 10°C$	6.28 ± 0.47 (61)	62	124	–
Skeletons§ in 5 mM salt ≤10 s after extraction, $T \leq 10°C$	8.50 ± 0.98 (35)	85	227	+
Skeletons§ in 5 mM salt ~1 min after extraction, $T \leq 10°C$	7.88 ± 0.62 (34)	78	195	+
Skeletons‖ in 0.5–2.0 mM salt ~1 min after extraction, $T \leq 10°C$	9.72 ± 1.06 (43)	97	297	+
Skeletons§¶ in 150 mM salt for ≤3 min, $T \leq 10°C$	5.67 ± 0.27 (6)	56	101	+
Skeletons§¶ in 1.5 M salt for ≤3 min, $T \leq 10°C$	4.33 ± 0.29 (22)	43	59	++
Skeletons§¶ in 1.5 M salt for ≥3 min, $T \leq 10°C$	3.67 ± 0.48 (35)	37	44	–
Skeletons§ in 5 mM salt ≤10 s after extraction, $T = 30°C$	7.99 ± 0.93 (12)	79	200	++
Skeletons§¶ in 1.5 M salt ≤1 min, $T = 30°C$	4.46 ± 0.27 (6)	44	63	++
Skeletons, bulk prepared, in 5 mM salt, $T \leq 10°C$	3.43 ± 0.25 (8)	34	37	–
Skeletons, bulk prepared, in 150 mM salt, $T \leq 10°C$	2.55 ± 0.29 (8)	25	20	–
Skeletons, bulk prepared, in 1.5 M salt, $T \leq 10°C$	2.56 ± 0.28 (6)	25	20	–

* Equivalent diameter ± SD (number of samples). See Materials and Methods. ‡Qualitative measure of flexibility, as judged by thermal undulation and deformation under flow. §Skeletons prepared in 5 mM Na-Phosphate buffer inside the flow chamber. ‖Skeletons prepared in 0.5–2.0 mM Na-Phosphate buffer inside the flow chamber. ¶Skeletons exposed to high salt within 3 min of extraction.

indented or convoluted shapes. Errors were computed as the standard deviation and reflect, apart from random experimental error, the size distribution of the population of cells. The equivalent surface area (Table 1) was computed as the surface area corresponding to a sphere of the equivalent diameter. Freshly extracted skeletons were nearly spherical and never strongly flattened, as was confirmed by a focal series through the images at zero flow rate. Note that any measurement based on optical sections is likely to underestimate the true surface area somewhat, since the light microscope cannot resolve subwavelength surface corrugations. Average tether lengths (spectrin tetramer end-to-end distances) were computed from the surface area, the known values for the number of tetramers per cell, and the connectivity of the skeletal network (Byers and Branton, 1986; Bennet, 1990). Because the surface area may be underestimated, the derived tether length probably represents a lower bound. Power-law fits were computed with software that uses the Levenberg-Marquardt algorithm, a standard nonlinear least-squares method.

Skeleton and bead preparation

Fresh blood was drawn from one of us (C.F.S. or K.S.), stored on ice in acid citrate dextrose, and used within 2 wk. Microscopic silica beads, ~0.5 μm diameter (a gift of Howard Berg, Harvard University; prepared according to Stöber et al., 1968), were nonspecifically bound to erythrocytes. These refractile beads served as "handles" that made it possible to maintain a cell—or, after extraction, its skeleton—in a fixed position, against the flow of medium, using optical tweezers.

Extraction of skeletons under the microscope

Red blood cells (RBCs) in a 100-μl sample were washed three times in 150 mM salt buffer. Washed, packed cells were diluted to 2×10^5 cells/μl with 150 mM salt buffer, and a 10-μl aliquot of these cells was incubated with 1 μl of a silica bead suspension (~10^6 beads/μl) for ~1 h on ice. Under these conditions, a single bead typically bound to each erythrocyte and remained bound to the cytoskeleton during subsequent lysis and detergent extraction. In most experiments, the bottom coverglass of the flow chamber was silanized (Prosil-28; PCR Inc., Gainesville, Florida), and, immediately before introducing the RBC sample, the assembled chamber was incubated with a buffer containing BSA (100 mg/ml). These treatments prevented both erythrocytes and ghosts from sticking to chamber surfaces but did not prevent the adhesion of freshly prepared skeletons. A 200-fold dilution of the RBC-bead solution was then pumped into the flow cell. Ghosts were prepared in situ by replacing the 150 mM salt buffer with 5 mM salt buffer. After thorough flushing with 5 mM salt buffer, a ghost with one bound bead was identified and trapped with the optical tweezers and then positioned near the center of the video field. Next, the chamber was flushed with 5 mM salt buffer containing detergent to extract lipid from the ghost, leaving behind the skeleton. Because salt-induced contraction was partly irreversible, some of the skeletons for the experiments of Fig. 6 were isolated at even lower salt concentrations (0.5, 1, or 2 mM). Isolated skeletons were observed for at most 1 h, during which all manipulations took place.

The shape of the flow chamber creates a laminar flow field that is unidirectional and parabolic (Berg and Block, 1984). The observation portion of the chamber has dimensions of $8 \times 8 \times 0.3$ mm. Near to the coverglass surface, the flow velocity increases linearly with height: at a distance of 10 μm above the cover glass, the local flow velocity, v (μm/s), is proportional to the volume flow rate, Q (μl/s), $v = aQ$, with $a \sim 1$ μm/μl for our chamber. Since the flow velocity in the vicinity of the skeleton was less than one tenth of the flow velocity in the center of the chamber, diffusion of ions from (or toward) the center limited the speed with which salt concentration could be changed. For $Q = 100$ μl/s, the maximal flow rate that allowed reliable trapping, we estimated that the salt concentration near the skeletons equilibrated within ~60 s after new buffer entered the flow cell.

Bulk extracted skeletons

RBC skeletons were prepared by standard methods (Sheetz and Sawyer, 1978; Shen et al., 1984) with the following modifications. Ghosts, prepared according to Dodge et al. (1963), were mixed with one volume of 5 mM salt buffer, containing 20% Triton X-100, at 18°C. After 5 min, a buffer containing 75 mM Na-phosphate and 3 M NaCl was added to achieve a final concentration of 25 mM Na-phosphate and 1 M NaCl. The samples were left for 50 min at 18°C and were then cooled to 4°C. Skeletons were separated from lipids and dissolved proteins by centrifugation through a 10–50% sucrose gradient containing 0.5% (wt/vol) Triton X-100, 25 mM Na-phosphate, and 1 M NaCl (100,000g, 40 min, 10°C). The skeletons, which accumulated at the bottom of the tube without forming aggregates, were resuspended in buffer (25 mM Na-phosphate and 1 M NaCl) containing 0.05% (wt/vol) Triton X-100 and then dialyzed overnight against this buffer.

RESULTS

Direct observation of RBC skeleton extraction

Ghosts were spherical in 5 mM salt buffer (Fig. 2 *a*, diameter $d = 6.28 \pm 0.47$ μm; for a summary of data, see

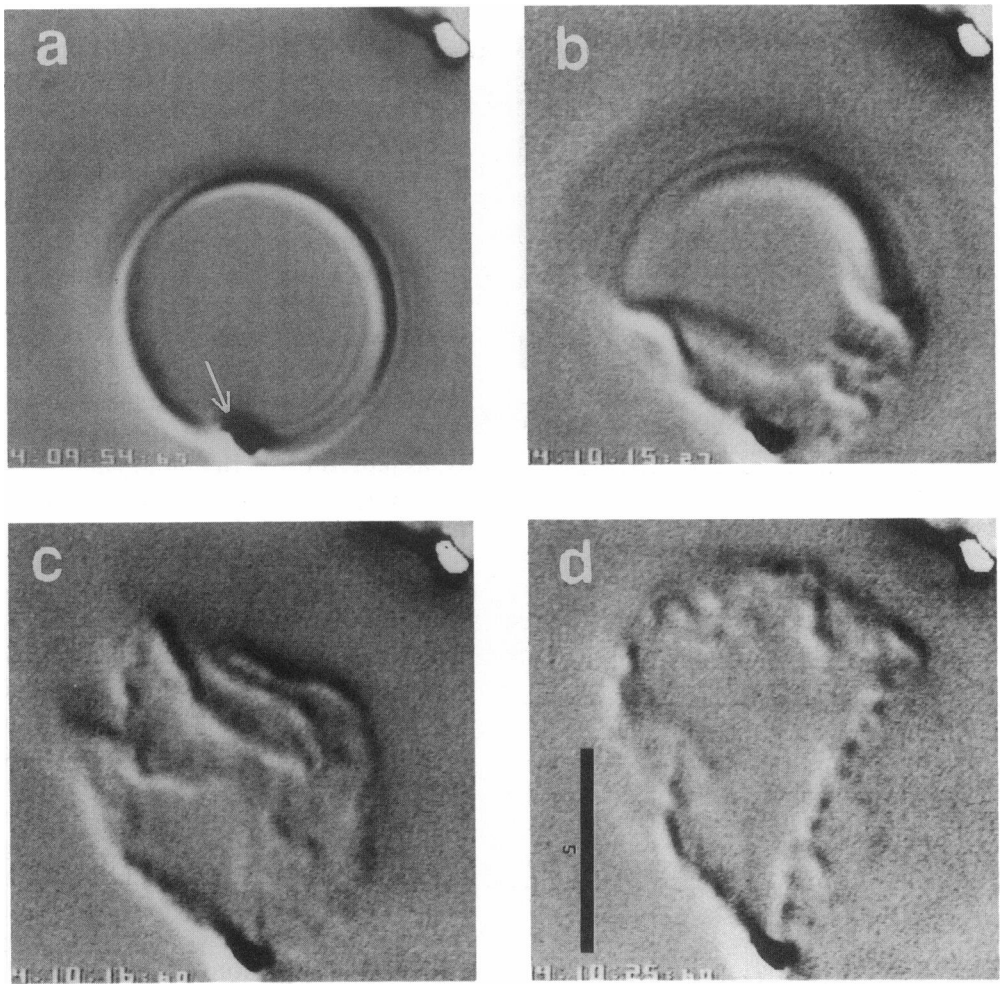

FIGURE 2 A video sequence showing the detergent extraction of an RBC skeleton at low temperature ($T < 10°C$), trapped by optical tweezers (buffer flow from bottom to top of image). Buffer flow orients the skeleton such that the central cross-section remains in focus. (*a*) An osmotically swollen ghost with a bound silica bead (*arrow*). (*b*) ~20 s later, detergent begins to dissolve the lipid bilayer. (*c*) ~1.5 s later, the expanding skeleton is released from the constraint of the bilayer. (*d*) ~10 s later, the fully extracted membrane skeleton appears. Pronounced folds and inhomogeneities in the network were typical (see also Fig. 4 *a*). Bar, 5 μm.

Table 1). With the arrival of detergent, the lipid membrane began to deform and then, within a second or so, the skeleton expanded as the lipid was dissolved (Fig. 2, *b–d*). Skeletons were far less refractile and ~35% larger than ghosts ($d = 8.50 \pm 0.98$ μm). This implies that for ghosts in 5 mM salt buffer, the skeleton exists in a lipid-imposed state of compression. The overall shape of the skeletons remained shell-like and roughly spherical, although persistent creases and folds were often apparent (Fig. 2 *d*). When the extraction was performed at low temperatures,[2] we consistently observed submicroscopic globular aggregates, or vesicles, attached to the skeletons (Fig. 3 *a*). Similar vesicles have been observed previously (Sheetz and Sawyer, 1978; Liu et al., 1987). The skeletons showed vigorous thermal (Brownian) fluctuations in shape. Within a minute or so after extraction, under continuing buffer flow, the diameter of the skeletons relaxed to ~93% of the size observed immediately after extraction ($d = 7.88 \pm 0.62$ μm). No further morphological or dynamical changes were noted when skeletons were held in the optical trap in flowing 5 mM salt buffer for up to 40 min.

We found no correlation between the shape of the extracted skeleton in 5 mM salt buffer and the shape of the parent RBC. Direct observation of the extraction process showed that static deviations from a spherical average shape were determined mainly by randomly occurring convolutions during the initial moments of extraction. Such convolutions (Fig. 2 *b*) were probably due to asymmetric or locally inhomogeneous insertion of detergent into the outer and inner leaflets of the lipid membrane. When large local membrane curvature occurred, distant parts of the membrane skeleton touched and then stuck

[2] To avoid condensation on the optics, we performed low temperature experiments at either 6, 8, or 10°C, depending on the relative humidity in the laboratory. The properties of skeletons at these three different temperatures appeared to be the same.

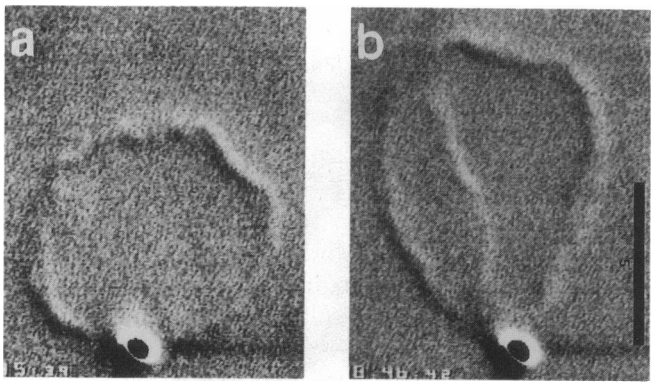

FIGURE 3 The elastic response of a freshly extracted skeleton to a small flow field at $T = 30°C$ (buffer flow from bottom to top of image). (*a*) Thermally fluctuating skeleton without buffer flow. (*b*) The same skeleton, deformed by ~40 μm/s flow. The skeleton in *b* assumed a rest shape indistinguishable from *a* within seconds after the flow was turned off. Note the more regular and spherical rest shape, as compared with the skeleton of Fig. 1, due to extraction at higher temperature. Bar, 5 μm.

to one another, leading to stable creases and folds (Fig. 2, *c* and *d*).

The isolated membrane skeletons were more flexible than either ghosts or intact RBCs: small stresses induced by a buffer flow of ~40 μm/s induced large deformations in freshly extracted skeletons (Fig. 3), whereas ghosts and RBCs showed no deformation under similar conditions.

Effects of ionic strength on freshly extracted skeletons

Individual membrane skeletons held with optical tweezers and extracted in 5 mM salt buffer were exposed to buffers containing increasingly higher salt. The following effects were noted (Fig. 4, *a–d*). (*i*) Skeletons shrank significantly, from $d = 8.50$ μm at 5 mM salt to $d = 4.33$ μm at 1.5 M salt (Table 1). Shrinkage also has been reported for bulk extracted skeletons (Johnson et al., 1980; Lange et al., 1982; Vertessy and Steck, 1989). (*ii*) At ~600 mM NaCl, particles, aggregates, or vesicles that had been attached to the skeletons detached and washed away. Electrophoretic profiles of extracted skeletons have shown previously that stripping skeletons at high salt concentration elutes accessory proteins, among them many transmembrane proteins (Sheetz 1979; Shen et al., 1986). (*iii*) As the particles detached at ~600 mM NaCl, folds and creases also relaxed (compare Fig. 4, *a* with *c*) and the skeletons transiently gained flexibility, but thereafter continued to shrink, while loosing flexibility, as judged by thermal undulations.

Attempts to reverse the salt-induced contraction of freshly extracted skeletons by reimmersion in 5 mM salt buffer revealed that structural rearrangements had occurred while the skeletons were in the shrunken state. After the shortest possible exposure time to 1.5 M salt buffer (1 min), skeletons had shrunk to 55% of their initial (preshrunken) diameter but fully recovered on reexpansion in 5 mM salt buffer. With longer exposures to 1.5 M salt buffer, this reexpandability decreased rapidly. After 15 min at 10°C in 1.5 M salt buffer, the skeletons had shrunk to 47% of their initial diameter but recovered to only 62% of their initial diameter (Fig. 5). We found that leaving skeletons in 5 mM salt buffer for up to 40 min before shrinkage and reexpansion did nothing to change their behavior when placed in higher salt buffer (Fig. 5). At temperatures below 10°C, thermal fluctuations on optical length scales died out completely within 1 h in 1.5 M salt buffer, and skeletons no longer deformed in response to flow fields. Such skeletons assumed irregular shapes that were quite similar to bulk extracted skeletons. The shrunken shapes of individual skeletons appeared to be unrelated to their earlier, ex-

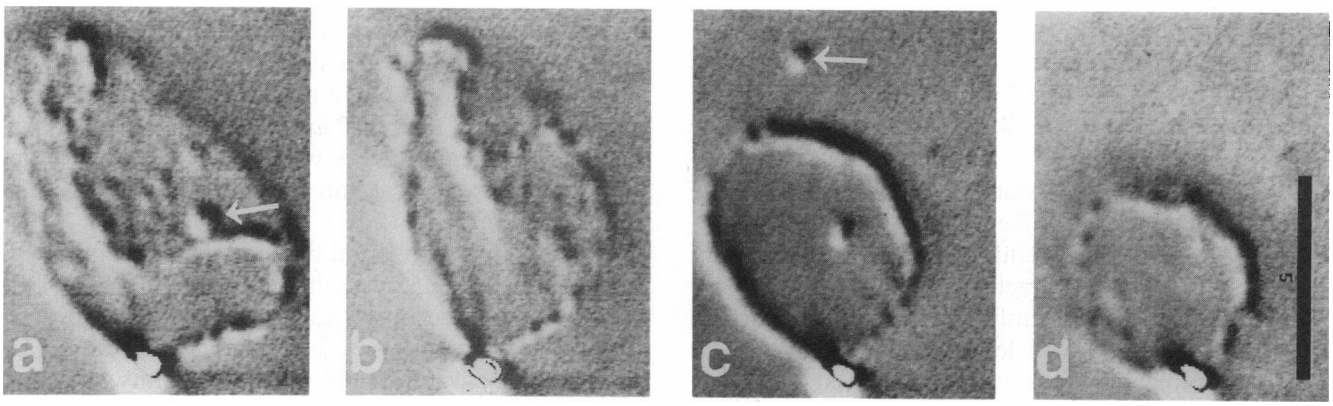

FIGURE 4 A video sequence illustrating the effect of increasing salt concentration on a freshly extracted skeleton at 6°C (buffer flow is from bottom to top of image). (*a*) A skeleton 22 s after detergent extraction in 5 mM salt buffer. Parts of the membrane skeleton have become cross-bonded to the opposite cell side during extraction, as evidenced by the pronounced fold. Arrow points to a submicron vesicle attached to the skeleton. (*b*) ~15 s later, unfolding in response to increasing salt concentration (from 5 mM to 1.5 M). (*c*) ~15 s later, submicron vesicles dissociate from the skeleton (*arrow*). (*d*) ~45 s later, the final state in 1.5 M salt. Bar, 5 μm.

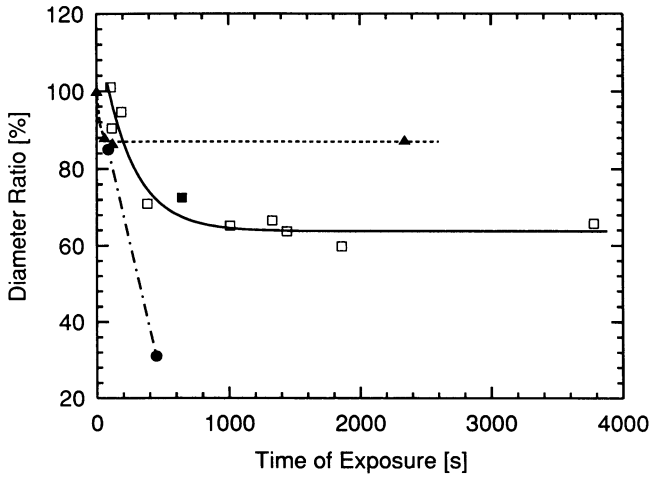

FIGURE 5 The time dependence of reversibility of salt-induced shrinkage of freshly extracted skeletons. Skeletons were prepared in 5 mM salt buffer, left for 1 min, then shrunk for varying lengths of time in a 1.5 M salt buffer (60–3,800 s). Subsequently, skeletons were reexpanded in a 5 mM salt buffer, and final diameters were measured. The plot shows the ratio of the final to the initial diameters (measured at t = 1 min after extraction) as a function of time of exposure to the higher salt (□, T < 10°C; ●, T = 30°C). One control skeleton was exposed to 1.5 M salt after 40 min 5 mM salt (■). The plot shows the ratio of its final diameter to the diameter measured at t = 40 min after extraction. Other control skeletons (T < 10°C) were maintained for up to 40 min in 5 mM salt buffer (▲). For these, the plot shows the ratio of the final to initial diameters (measured at $t \sim$ 10 s after extraction) as a function of time. In the experiments shown in this figure, diameters were not derived from the circumferences but were measured directly. Lines serve only to guide the eye.

panded shapes observed in 5 mM salt buffer. At 30°C, skeletons became rigid within minutes in 1.5 M salt buffer. The loss of reexpandability occurred much more rapidly at 30°C and thus seemed to be thermally activated.

The surface area of skeletons that had been extracted in 5 mM salt buffer and subsequently transferred to 150 mM salt buffer was 101 ± 10 μm^2, only slightly less than the ghost surface area of 123 ± 17 μm^2 (Table 1). This implies that lateral tension in the skeleton in vivo is close to zero. Other investigators, studying bulk extracted skeletons with substantially smaller surface areas, have postulated a nonzero tension (Kozlov and Markin, 1987, 1990; Steck, 1989).

To quantify the elastic properties of freshly extracted skeletons, we measured their diameters while washing with buffers whose salt concentration was increased stepwise from 0.5 mM to 1.5 M (Fig. 6). The diameter of the skeletons reached a maximal value of 9.72 ± 1.06 μm at salt concentrations below 2 mM. Between 2 and 100 mM, the diameter, d, approximately obeyed the power law

$$d \propto c^{-\alpha}, \qquad (1)$$

where $\alpha = 0.13 \pm 0.01$ and c is the salt concentration. For concentrations exceeding 100 mM, skeleton size remained constant until, at ~600 mM (concurrent with the detachment of the small adhering vesicles), skeletons shrank further.

Effects of ionic strength on bulk prepared skeletons

For comparison, we also studied the response to changing ionic strength of bulk extracted skeletons prepared in 1 M salt more than 24 h before an experiment (Fig. 7). Their average diameters were roughly half those of freshly extracted skeletons, and thermal fluctuations were never observed (Table 1). In contrast to freshly extracted skeletons, which tended to spread out and stick to coverglass surfaces, bulk extracted skeletons attached to the coverglass only over a very small contact area, a further indication of their rigidity. Salt-induced size changes could therefore be measured with coverglass-at-

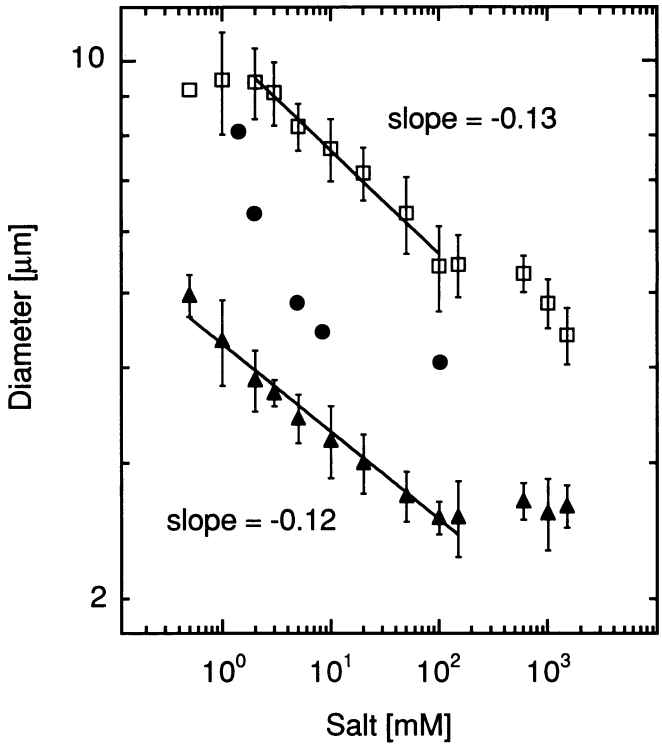

FIGURE 6 The dependence of the diameter of the equivalent sphere on salt concentration at low temperature (T < 10°C). □, freshly extracted skeletons. Skeletons were extracted with 0.5, 1, 2, or 5 mM salt buffer; the salt concentration was then rapidly raised stepwise up to 1.5 M (time per step, ~120 s). Points are averages over runs with nine individual skeletons; no systematic differences due to the different initial salt concentrations were found. ▲, bulk extracted skeletons. Data for the different salt concentrations were not taken in a monotonic sequence; ionic strength was first lowered, raised, then lowered again as points were collected in different regions of the curve. No hysteresis (systematic deviation from a single curve) was noted; this constitutes evidence for reversible shrinkage. Points are averages for eight individual skeletons that were monitored simultaneously. ●, radius of gyration of isolated spectrin dimers, measured by static light scattering (data adapted from Elgsaeter, 1978, and scaled by a constant factor).

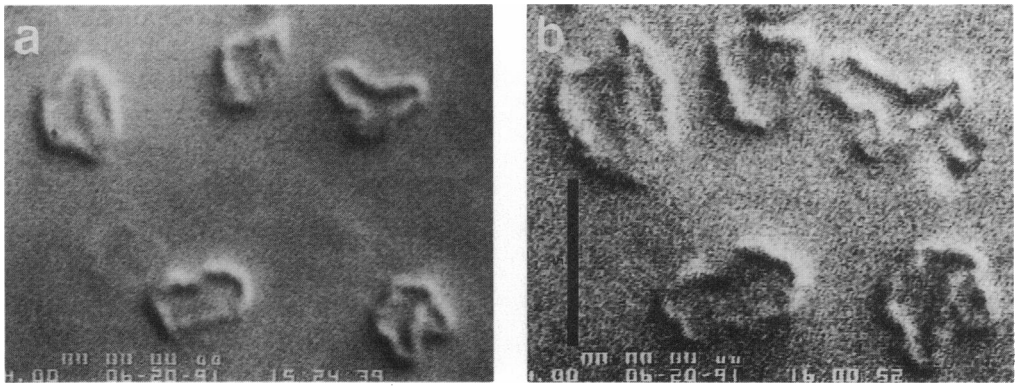

FIGURE 7 Bulk-extracted skeletons at low temperature (T = 10°C) attached to the coverglass surface of the flow chamber and subsequently exposed to buffers of varying salt concentration. (*a*) Skeletons in 1 M salt. (*b*) Skeletons in 2 mM salt. Note that skeletons change in size but conserve their shape under variations of salt concentration. Bar, 5 μm.

tached skeletons, without the need for optical tweezers. These skeletons did not deform in buffer flow of ~40 μm/s and the creases, folds, and overall contours were strikingly conserved as they shrank and reexpanded in response to changing salt. Between 1 and 100 mM salt, diameters obeyed Eq. 1, with $\alpha = 0.12 \pm 0.01$ (Fig. 6). At 100 mM salt, the induced shrinkage reached a plateau that persisted up to the highest salt concentrations (1.5 M). Although half the size of freshly extracted skeletons, the diameters of bulk extracted skeletons responded in a reversible fashion even after prolonged incubation in 1.5 M salt buffer.

Rearrangement of the membrane skeleton in ghosts

To determine if structural changes similar to those that inhibited reexpansion could occur even before lipid extraction, we prepared skeletons from osmotically collapsed ghosts that had been incubated with 5 mM salt buffer containing 400 mM sucrose for 40 min at 10°C. Osmotic collapse caused the opposed cytoplasmic surfaces of the cell membrane to touch (Fig. 8 *a*). Skeletons produced by subsequent detergent extraction preserved the cup-shaped form of the ghosts, with opposing surfaces connected (Fig. 8 *b*). These shapes were conserved through salt induced shrinkage (data not shown). Thus, even in the presence of the lipid membrane, bringing regions of the membrane skeleton into apposition can induce structural rearrangements.

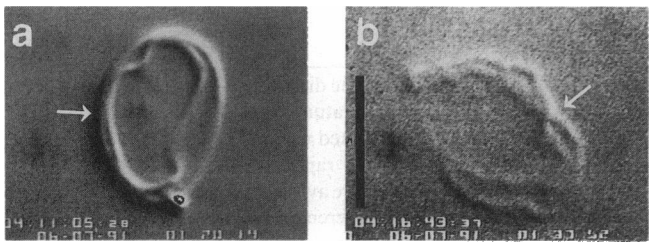

FIGURE 8 Detergent extraction of an osmotically collapsed ghost at low temperature (5 mM salt buffer, 400 mM sucrose, T = 10°C). (*a*) Cross-section through the cup-shaped collapsed ghost. Opposing faces of the membrane were very close (*arrow*). (*b*) Skeleton extracted from the same ghost. The cup shape was conserved. Opposing surfaces of the skeleton were cross-bonded (*arrow*) and did not dissociate during salt-induced shrinkage (data not shown). Bar, 5 μm.

DISCUSSION

Freshly extracted membrane skeletons are remarkably flexible structures. The large amplitudes of thermal undulations, as well as the high deformability in response to small shear forces (Fig. 3), indicate that isolated skeletons have a markedly smaller bending elastic constant than the composite membrane consisting of both lipid bilayer and skeleton. A small bending rigidity for the skeleton is not surprising. Analysis of thermal fluctuations shows that RBC membranes can have even smaller bending elastic constants than single-component lipid bilayers alone (Duwe et al., 1989). Since a fluid lipid bilayer cannot support shear strain, the shear elasticity of RBCs must be attributable to the skeleton. Although we did not quantify the shear modulus, we observed a large pliability in response to the small shear forces (~pN) applied with optical tweezers. This is consistent with a low upper bound for the shear elastic constant, as found in a recent study of long wavelength, thermally excited "flicker" excitations of whole RBCs (Peterson et al., 1992).

The changes that take place in freshly extracted skeletons could account for previous reports of rigid isolated skeletons. Membrane skeletons are flexible and nearly spherical immediately post extraction and remain flexible, albeit transiently, even when placed in high ionic strength buffer. But, in high ionic strength, rearrangements are rapid: within minutes after inducing shrinkage by screening electrostatic repulsion with salt, shrinkage becomes irreversible (Fig. 5). We found no evidence for

static shape memory in freshly extracted skeletons of normal cells. Thus, the resting shape of RBCs cannot be imposed by the membrane skeleton alone. Static shape irregularities, which we observed more frequently at low temperatures than at 30°C, were transient and determined by random convolutions during the first stages of lipid-detergent mixing, when distal parts of the skeleton became attached.

We suggest that the changes that transform freshly extracted skeletons into irreversibly rigid, irregular shapes are attributable to the formation of new spectrin dimer-dimer bonds, so as to convert the native two-dimensional network into a weakly three-dimensional structure. The equilibrium between dimers and tetramers is strongly dependent on ionic strength, favoring dimers at low salt concentrations and tetramers at physiological and higher salt concentrations (Ungewickell and Gratzer, 1978). Although, in ghosts, spectrin is primarily in the form of tetramers, a small but significant fraction remains in the form of dimers (Liu and Palek, 1980). A comparable fraction of spectrin is expected to be in dimer form in skeletons prepared in 5 mM salt buffer. Raising the salt concentration has two effects: electrostatic repulsion is screened, causing the skeletons to shrink, and the equilibrium between dimers and tetramers is shifted toward tetramers, as dimers associate. Because it is likely that the shrunken skeleton is locally convoluted (the freshly isolated skeleton has low bending rigidity), the probability is high that some of the newly formed links will form out-of-plane connections, producing a weakly three-dimensional network. We note that only a few out-of-plane connections, enough to stabilize corrugations, are needed to enhance the rigidity of the entire structure and account for the diminished flexibility. Similar linkages between distant regions of the skeleton apparently formed when normally distant cytoplasmic faces of the cell membrane were brought into contact with each other by osmotically collapsing intact ghosts (Fig. 8). Spectrin cross-linking events have been used to explain changes in whole RBCs after denaturing treatments (Bull, 1988; Fischer, 1988), prolonged ATP depletion (Fischer, 1988), and mechanical overstressing (Bull et al., 1986). Dynamic cross-linking may also account for irreversibly sickled cells in persons with sickle cell anemia (Lux et al., 1976; Liu et al., 1991).

This cross-linking scenario assumes that, in vivo, the membrane skeleton maintains its entirely two-dimensional connectivity through multiple attachments to the smooth lipid bilayer. Once the lipid bilayer is removed, entropic forces will tend to drive connectivity in such a way as to promote a three-dimensional network. Salt treatment leads to an irreversible stiffening of the membrane skeleton, because even when the salt is removed, there is no force to drive connectivity to reform a two-dimensional network.

Our measurements of salt-dependent diameter changes of fresh and aged skeletons can be used to deduce elastic properties of spectrin. Shrinkage of the flexible spectrin network might result from large-scale conformational changes in the network, such as crumpling or folding (see below and Nelson et al., 1989), or from small-scale changes in the spectrin end-to-end length. The crumples and folds of rigidified, bulk extracted skeletons were conserved right down to the resolution limit of the microscope, ~300 nm (Fig. 7). The meshwork size of the spectrin network is only slightly smaller than this, varying between 50 and 200 nm. Hence, in rigidified skeletons, salt dependent size changes appear to be mainly due to variation in the spectrin end-to-end distance. The same change in end-to-end distance explains the shrinkage of freshly extracted skeletons, because their diameters scale in the same way with salt concentration (Fig. 6). In support of this view, static light scattering measurements of the salt-dependent radius of gyration of isolated spectrin dimers have shown that the relative change in dimer length parallels the relative change in skeleton diameter (Elgsaeter, 1978) (see also Fig. 6).

Both electron microscopy (Shotton et al., 1979) and viscometry (Stokke et al., 1985) suggest that spectrin, in solution, behaves like a worm-like random chain. The average conformation and elastic properties of such molecules are characterized by a persistence length, l_p (de Gennes, 1979; Flory, 1988). Assuming a qualitatively similar behavior for spectrin in the skeleton and using the salt response curves (Fig. 6), we can arrive at a rough estimate of the persistence length of spectrin in situ. This is significant, because spectrin in the skeleton might have different elastic properties from spectrin in solution (McGough and Josephs, 1990). The total persistence length, l_p, is the sum of a salt-dependent (extrinsic) contribution, l_e, due to electrostatic repulsion, and a salt-independent (intrinsic) contribution, l_i, due to stereochemical constraints (Odijk and Houwaart, 1978). Because l_e decreases with increasing ionic strength (charge screening), whereas l_i remains constant, one expects a leveling off of the salt response curve when l_e is comparable with l_i. For our data, this crossover occurs near 100 mM salt (see Fig. 6). Le Bret (1982) numerically computed l_e for a variety of parameters (average axial charge separation, molecular radius, ionic strength, etc.). For a spectrin-like molecule at 100 mM salt, we estimate from his results that $l_e \approx 3$ nm (choosing the cross-sectional radius = 2.5 nm, axial charge separation = 0.4 nm, Debye screening length = 1 nm; see Table 2, Le Bret, 1982). The persistence length of spectrin at this salt concentration is therefore $l_p = 2l_e \approx 10$ nm, which corresponds to about two segments (i.e., units of the repeating structural motif) of the spectrin molecule (Speicher and Marchesi, 1984). Studies of isolated spectrin dimers using viscometric techniques yield a similarly small value for l_p (20 nm) (Stokke et al., 1985). The average end-to-end distance, R_{ee}, can be calculated from the persistence length, l_p, and the spectrin contour length, L, as $R_{ee} = \sqrt{2l_p(L - l_p)}$, for wormlike chains of sufficient length (Flory, 1988).

For l_p = 10 nm and L = 200 nm, $R_{ee} \approx$ 60 nm, a value that is comparable with the average tether lengths of Table 1 (e.g., 56 nm at 150 mM NaCl). The persistence length derived from our salt response curves is, admittedly, a crude estimate, but the significance of the number is related to its smallness (a few nanometers) and not to the exact value. A short persistence length is consistent with the notion that the conformational entropy of spectrin is the basis of the shear elasticity of the composite erythrocyte membrane (Waugh and Evans, 1979; Elgsaeter et al., 1986).[3]

A theoretical model for salt-induced size changes in skeletons has been used to derive a scaling exponent of $\alpha = 1/8$ for Eq. 1 (Kozlov and Markin, 1987, 1990), quite close to our experimental value, 0.13. This model assumes that the isolated skeleton is electrically homogeneous on a scale set by the Debye screening length and that the effective skeleton thickness is small compared with this Debye length. But the Debye length varies from ~1 nm, in 100 mM salt (a distance even smaller than the thickness of a spectrin molecule), to ~10 nm, in 1 mM salt (Landau and Lifshitz, 1980). Since the charged protein constituents of the skeleton are arranged in a triangulated network whose interstices span from tens to hundreds of nanometers and whose thickness exceeds 10 nm, it seems implausible that the particular assumptions of the Kozlov and Markin model can be correct.

Irrespective of modeling, our finding that dynamic alterations in structure occur soon after extraction, with concomitant changes in elasticity, indicates that experimental determinations of skeleton properties must be made rapidly if they are to be meaningful. New tools, such as high resolution video microscopy, in combination with optical tweezers, offer an attractive means for further, more quantitative study of these labile structures.

We thank Howard Berg for silica beads, Bruce Schnapp for the loan of a Peltier temperature stage, Daniel Kiehart for the loan of a microscope used in the early stages of this work, Jay Scarpetti for help with printing the figures, and Arnljot Elgsaeter, Erwin Frey, and David Nelson for encouragement and helpful discussions.

This work was supported by grants from the National Institutes of Health (K.S., Biophysics Training Grant; D.B., HL-17411), the Deutsche Forschungsgemeinschaft (C.F.S.), and by the Rowland Institute for Science (K.S., S.M.B.).

Received for publication 13 January 1992 and in final form 16 April 1992.

[3] The bending stiffness of the spectrin skeleton is determined by the arrangement and elastic properties of its network tethers. On a length scale larger than the network mesh size, it is meaningful to discuss bending stiffness as a continuum parameter. Unlike linear polymers, where bending stiffness is scale independent and determined by short range interactions between neighbors, the bending stiffness in a polymer network can be scale dependent, diverging at long length scales. This effect has been predicted for networks of freely jointed monomers (Nelson and Peliti, 1987; Nelson et al., 1989) and appears to be insensitive to the particular network symmetry. Here, the nearly spherical shapes adopted by freshly extracted skeletons imply large-scale correlations in average surface orientation, over distances of micrometers. Because of this scale-dependent stiffness, such large-scale correlations are consistent with a network comprised entirely of flexible connections. Theory also predicts that the in-plane shear and compressional elastic moduli of these networks ought to decrease with increasing length scale (Aronovitz and Lubensky, 1988), a property that might explain the very small shear elastic constants that have been postulated for RBC skeletons (Fischer et al., 1978, 1981; Peterson et al., 1992).

REFERENCES

Aronovitz, J. A., and T. C. Lubensky. 1988. Fluctuations in solid membranes. *Phys. Rev. Lett.* 60:2634–2637.

Ashkin, A., J. M. Dziedzic, J. E. Bjorkholm, and S. Chu. 1986. Observation of a single-beam gradient force optical trap for dielectric particles. *Optics Lett.* 11:288–290.

Bennett, V. 1990. Spectrin-based membrane skeleton: a multipotential adaptor between plasma membrane and cytoplasm. *Physiol. Rev.* 70:1029–1065.

Berg, H. C., and S. M. Block. 1984. A miniature flow cell designed for rapid exchange of media under high-power microscope objectives. *J. Gen. Microbiol.* 130:2915–2920.

Block, S. M. 1990. Optical tweezers: a new tool for biophysics. *In* Noninvasive Techniques in Cell Biology. K. J. Foskett and S. Grinstein, editors. Wiley/Liss, New York. 375–402.

Block, S. M., K. A. Fahrner, and H. C. Berg. 1991. Visualization of bacterial flagella by video-enhanced light microscopy. *J. Bacteriol.* 173:933–936.

Bull, B. S. 1988. The cross-bonding phenomenon and studies of red cell deformability. *Blood Cells NY.* 13:395–396.

Bull, B. S., R. S. Weinstein, and R. A. Korpman. 1986. On the thickness of the red cell membrane skeleton: quantitative electron microscopy of maximally narrowed isthmus regions of intact cells. *Blood Cells NY.* 12:25–42.

Byers, T. J., and D. Branton. 1986. Visualization of the protein associations in the erythrocyte membrane skeleton. *Proc. Natl. Acad. Sci. USA.* 82:6153–6157.

Chasis, J. A., and N. Mohandas. 1986. Erythrocyte membrane deformability and stability: two distinct membrane properties that are independently regulated by skeletal protein associations. *J. Cell Biol.* 103:343–350.

de Gennes, P.-G. 1979. Scaling Concepts in Polymer Physics. Cornell University Press, Ithaca, NY. 21 pp.

Dodge, J. T., C. Mitchell, and D. J. Hanahan. 1963. The preparation and chemical characteristics of hemoglobin-free ghosts of human erythrocytes. *Arch. Biochem. Biophys.* 100:119–130.

Duwe, H. P., K. Zeman, and E. Sackmann. 1989. Bending undulations of lipid bilayers and the red blood cell membrane: a comparative study. *Prog. Colloid. Polym. Sci.* 79:6–10.

Elgsaeter, A. 1978. Human spectrin 1: a classical light scattering study. *Biochim. Biophys. Acta.* 536:235–244.

Elgsaeter, A., B. T. Stokke, A. Mikkelsen, and D. Branton. 1986. The molecular basis of erythrocyte shape. *Science (Wash. DC).* 234:1217–1223.

Evans, E. A. 1973. New membrane concept applied to the analysis of fluid shear- and micropipette-deformed red blood cells. *Biophys. J.* 13:941–954.

Fischer, T. M. 1988. Role of spectrin in cross bonding of the red cell membrane. *Blood Cells NY.* 13:377–394.

Fischer, T. M., M. Stöhr-Liesen, and H. Schmid-Schönbein. 1978. The

red cell as a fluid droplet: tank tread-like motion of the human erythrocyte membrane in shear flow. *Science (Wash. DC).* 202:894–896.

Fischer, T. M., C. W. M. Haest, M. Stöhr-Liesen, H. Schmid-Schönbein, and R. Skalak. 1981. The stress-free shape of the red blood cell membrane. *Biophys. J.* 34:409–422.

Flory, P. J. 1988. Statistical Mechanics of Chain Molecules. Hanser Publishers, New York. The Oxford University Press, New York. 401 pp.

Johnson, R. M., G. Taylor, and D. B. Meyer. 1980. Shape and volume changes in erythrocyte ghosts and spectrin-actin networks. *J. Cell Biol.* 86:371–376.

Kozlov, M. M., and V. S. Markin. 1987. Model of red blood cell membrane skeleton: electrical and mechanical properties. *J. Theor. Biol.* 129:439–452.

Kozlov, M. M., and V. S. Markin. 1990. Model of red blood cell membrane skeleton. *In* Contemporary Problems of Biomechanics. G. G. Cherbnyi and S. A. Regirer, editors. CRC Press, Boca Raton, FL. 11–54.

Landau, L. D., and E. M. Lifshitz. 1980. Statistical Physics. Pergamon Press, Oxford. 239 pp.

Lange, Y., R. A. Hadesman, and T. L. Steck. 1982. Role of reticulum in the stability and shape of the isolated human erythrocyte membrane. *J. Cell Biol.* 92:714–721.

Le Bret, M. 1982. Electrostatic contribution to the persistence length of a polyelectrolyte. *J. Chem. Phys.* 76:6243–6255.

Liu, S. C., and J. Palek. 1980. Spectrin tetramer-dimer equilibrium and the stability of erythrocyte membrane skeletons. *Nature (Lond.).* 285:586–588.

Liu, S. C., L. H. Derick, and J. Palek. 1987. Visualization of the hexagonal lattice in the erythrocyte membrane skeleton. *J. Cell Biol.* 104:527–536.

Liu, S. C., L. H. Derick, S. Zhai, and J. Palek. 1991. Uncoupling of the spectrin-based skeleton from the lipid bilayer in sickled red cells. *Science (Wash. DC).* 252:574–576.

Lux, S. E., K. M. John, and M. J. Karnovsky. 1976. Irreversible deformation of the spectrin-actin lattice in irreversibly sickled cells. *J. Clin. Invest.* 58:955–963.

McGough, A. M., and R. Josephs. 1990. On the structure of erythrocyte spectrin in partially expanded membrane skeletons. *Proc. Natl. Acad. Sci. USA.* 87:5208–5212.

Nelson, D. R., and L. Peliti. 1987. Fluctuations in membranes with crystalline and hexatic order. *J. Physique II (Paris).* 48:1085–1092.

Nelson, D. R., T. Piran, and S. Weinberg, editors. 1989. Statistical Mechanics of Membranes and Surfaces. World Scientific, Singapore.

Odijk, T., and A. C. Houwaart. 1978. On the theory of the excluded-volume effect of a polyelectrolyte in a 1-1 electrolyte solution. *J. Polym. Sci.* 16:627–639.

Peterson, M. A., H. Strey, and E. Sackmann. 1992. Theoretical and phase contrast microscopic eigenmode analysis of erythrocyte flicker: 1. amplitudes. *J. Physique II (Paris).* 2:1273–1285.

Sheetz, M. P. 1979. Integral membrane protein interaction with triton cytoskeletons of erythrocytes. *Biochim. Biophys. Acta.* 557:122–134.

Sheetz, M. P., and D. Sawyer. 1978. Triton shells of intact erythrocytes. *J. Supramol. Struct.* 8:399–412.

Shen, B. W., R. Josephs, and T. L. Steck. 1984. Ultrastructure of unit fragments of the skeleton of the human erythrocyte membrane. *J. Cell Biol.* 99:810–821.

Shen, B. W., R. Josephs, and T. L. Steck. 1986. Ultrastructure of the intact skeleton of the human erythrocyte membrane. *J. Cell Biol.* 102:997–1006.

Shotton, D. M., B. E. Burke, and D. Branton. 1979. The molecular structure of human erythrocyte spectrin. *J. Mol. Biol.* 131:303–332.

Speicher, D. W., and V. T. Marchesi. 1984. Erythrocyte spectrin is comprised of many homologous triple helical segments. *Nature (Lond.).* 311:177–180.

Steck, T. L. 1989. Red cell shape. *In* Cell Shape: Determinants, Regulation and Regulatory Role. W. Stein and F. Bonner, editors. Academic Press, Inc., New York. 205–246.

Stöber, W., A. Fink, and E. J. Bohn. 1968. Controlled growth of monodisperse silica spheres in the micron size range. *J. Coll. Interface Sci.* 26:62–69.

Stokke, B. T., A. Mikkelsen, and A. Elgsaeter. 1985. Human erythrocyte spectrin dimer intrinsic viscosity: temperature dependence and implications for the molecular basis of the membrane free energy. *Biochim. Biophys. Acta.* 816:102–110.

Ungewickell, E., and W. Gratzer. 1978. Self-association of human spectrin. *Eur. J. Biochem.* 88:379–385.

Vertessy, B. G., and T. L. Steck. 1989. Elasticity of the human red cell membrane skeleton. *Biophys. J.* 55:255–262.

Waugh, R. E. 1987. Effects of inherited membrane abnormalities on the viscoelastic properties of erythrocyte membranes. *Biophys. J.* 51:363–369.

Waugh, R. E., and P. Agre. 1988. Reductions of erythrocyte membrane viscoelastic coefficients reflect spectrin deficiencies in hereditary spherocytosis. *J. Clin. Invest.* 81:133–141.

Waugh, R. E., and E. A. Evans. 1979. Thermoelasticity of red blood cell membrane. *Biophys. J.* 26:115–132.

Yu, J., D. A. Fischman, and T. L. Steck. 1973. Selective solubilization of proteins and phospholipids from red blood cell membranes by nonionic detergents. *J. Supramol. Struct.* 1:233–248.